The 2025 IEEE Signal Processing in Medicine and Biology Symposium

Temporal *Imax*-Derived FOD Radiomics for Classification of Breast Cancer Treatment Response: A 4D DCE-MRI Study

Priyadharshini. B*, Mythili A*, Anandh K R**
***School of Electronics Engineering, Vellore Institute of Technology, Vellore, Tamil Nadu, India.**
****Department of Radiology, Cincinnati Children's Hospital Medical Center, Cincinnati, United States**

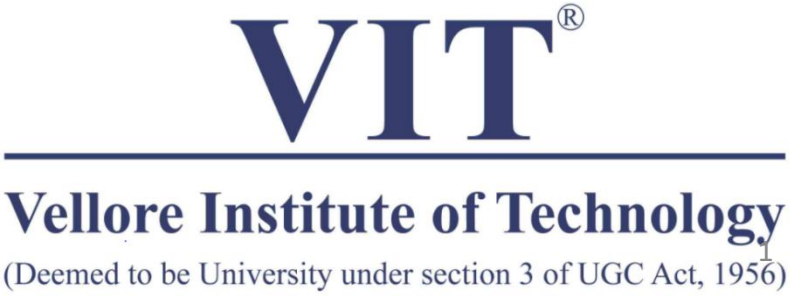

Introduction

Breast Cancer Facts - By the year 2020 to 2040, the World Health Organization (WHO) intends to avert 2.5 million breast cancer fatalities.

Causes of Breast cancer- Genetic, Environment, Earl menstruation, and Late menopause.

Breast Anatomy- Parts-Ducts, Lobes, Lobules, Lymp node.

DCE MRI for breast imaging produces high-resolutio images for women at high risk of breast cancer and also effective for evaluating dense female breasts

- Detect microscopic lesions in a (potentially) larg volume of tissue. High temporal resolution while preserving high spatial resolution.

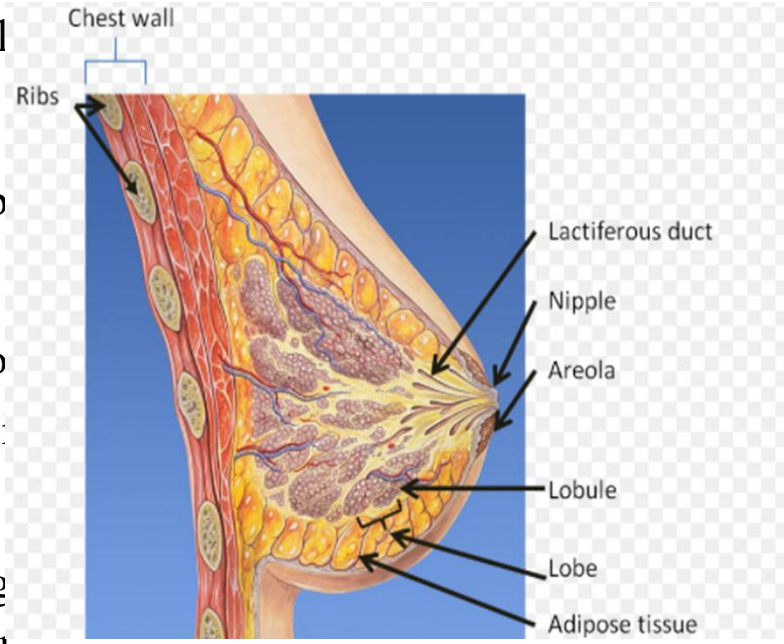

Introduction

- **Pathological Complete Response (pCR)**

pCR means no residual invasive cancer is found in the breast or lymph nodes after neoadjuvant chemotherapy.

- **Non-Pathological Complete Response (non-pCR)**

Non-pCR means residual invasive cancer is still present after treatment.

Introduction

Why classify patients into pCR and non-pCR?

- Helps oncologists evaluate treatment effectiveness early.
- Assists in personalizing therapy for breast cancer patients.

pCR classification supports

- Early de-escalation of therapy (reduce toxicity)
- Decision-making for breast conservation surgery

Non-pCR classification supports

- Therapy modification
- Predicting high-risk outcomes
- More aggressive monitoring

Motivation

- Breast cancer treatment response prediction remains challenging.
- Conventional DCE-MRI features often fail to capture microstructural variations.
- Fractional-order derivatives (FODs) provide enhanced textural and edge information
- Radiomics combined with temporal Imax maps can convert complex tumor behavior into quantifiable biomarkers
- Accurate classification of pCR vs non-pCR supports personalized therapy

Objectives

- To compute temporal *Imax* maps from 4D DCE-MRI and characterize perfusion-driven tumor heterogeneity.
- To generate fractional-order derivative (FOD) gradient images that enhance microstructural and kinetic variations within the tumor.
- To extract comprehensive radiomic features from FOD-transformed tumor regions for both treatment cycles (Visit 1, Visit 2, and Δ).
- To perform robust feature selection using LASSO to identify the most discriminative biomarkers for classifying pCR and non-pCR.
- To evaluate multiple machine-learning classifiers (SVM, Logistic Regression, Random Forest) using LOOCV and validate their ability to accurately predict treatment response.

Background

- DCE-MRI captures voxel-wise temporal enhancement
- Tumors have fractal, heterogeneous microstructures → FODs model them better than integer derivatives.
- Captures subtle perfusion changes, edge irregularities, and micro-textures hidden in Imax maps.
- Enhances tumor heterogeneity representation essential for pCR vs non-pCR discrimination.
- Provides multi-scale sensitivity (both fine and coarse tumor features).
- Improves radiomic feature contrast, leading to better classification performance.

Dataset & Imaging Protocol

- The dataset utilized for this analysis is adopted from the Cancer Image Archive (TCIA) repository.
- The QIN Breast DCE-MRI consists of 10 patients, each scanned at 32 time points for two Visits (V1 and V2), forming a 4D DCE-MRI.

Table 1. Dataset and image acquisition parameters

Parameter Name	Parameter Values
Image Strength (Patients)	10
Scanner	Siemens 3T
Sequence	TWIST
TR (ms)	2.9
TE (ms)	6.2
Flip Angle (degree)	10
FOV (mm)	300–340
Slice Thickness (mm)	1.4
Image Dimensions	320 × 320
Slice Number	112–120

Methodology

***Imax* map Calculation:**

$$I_{max}(x, y, z) = \max_{t} I(x, y, z, t) \qquad (1)$$

Fractional order derivative (FOD) gradient image:

- $D_x^{\alpha} f(x, y, z) = \sum_{k=0}^{n} (-1)^k \binom{\alpha}{k} f(x - k, y, z)$ (2)
- $D_y^{\alpha} f(x, y, z) = \sum_{k=0}^{n} (-1)^k \binom{\alpha}{k} f(x, y - k, z)$ (3)
- $D_z^{\alpha} f(x, y, z) = \sum_{k=0}^{n} (-1)^k \binom{\alpha}{k} f(x, y, z - k)$ (4)

Where, $\binom{\alpha}{k} = \frac{\Gamma(\alpha+1)}{\Gamma(k+1)\Gamma(\alpha-k+1)}$

'α' controls the differentiation order and 'k' indexes the discrete neighborhood contribution. Grünwald–Letnikov fractional derivative applied in X,Y,Z with 3×3×3 masks. **(α=0.5 used).**

Methodology

Mask Generation

- The tumor region from the breast DCE-MRI is extracted by an analytical segmentation model, named as Bezier-tuned Energy Functionals optimized via variational minimax for Volumetric Breast Tumor Segmentation (BEFVBTS) .

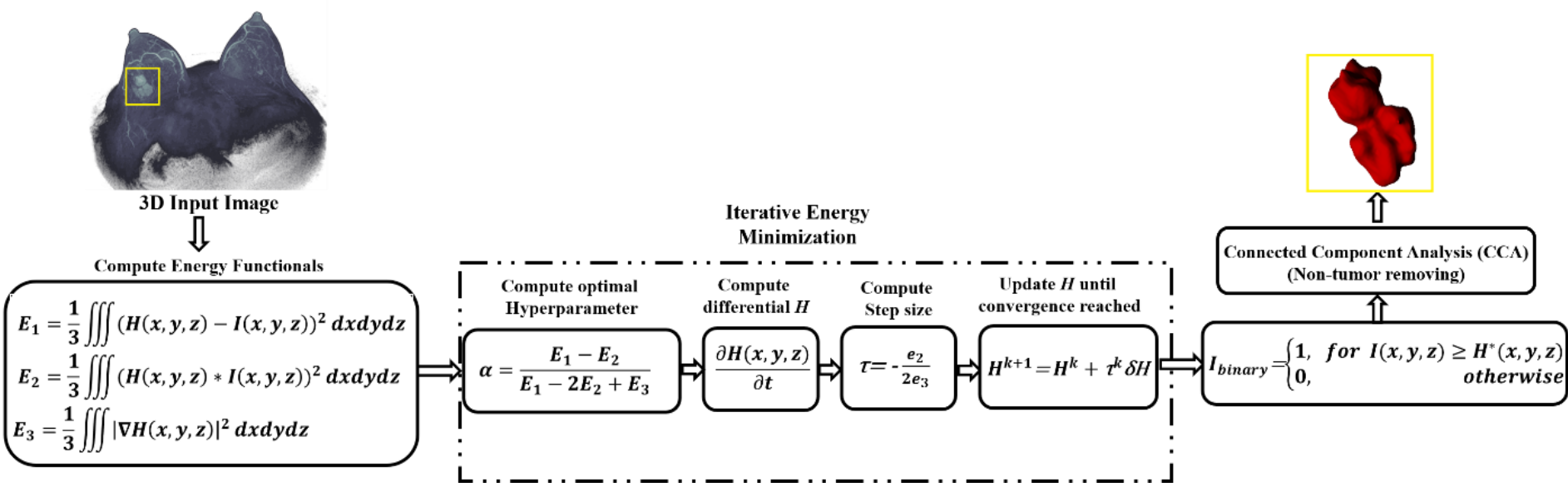

Figure 1. BEFVBTS model for tumor Segmentation and mask generation

Methodology

Feature Extraction:

- From the resulting ROI, a total of 572 radiomics features from 2 different classes (FOD and Log filtered image) were extracted for 2 cycles of chemotherapy.
- Pyradiomics, an open source, is engaged in extracting first-order, shape, and texture features from the transformed tumor region.

Feature Selection

- The LASSO (Least Absolute Shrinkage and Selection Operator) model is utilized to select the most significant features.

Methodology

Classification Models

- SVM and its variants, Logistic Regression, and Random Forest, are trained and tested by the selected optimal features. Leave-One-Out Cross-Validation (LOOCV) is employed to ensure robust and unbiased performance estimation

Performance Metrics

$$Accuracy = \frac{TP + TN}{TP + TN + FP + FN} \quad (5)$$

$$F1 - score = \frac{2TP}{2TP + FP + FN} \quad (6)$$

$$Precision = \frac{TP}{TP + FP} \quad (7)$$

$$Recall = \frac{TP}{TP + FN} \quad (8)$$

- TP- True Positive, TN- True Negative, FP- False Positive, and FN-False Negative.

Results and Discussion

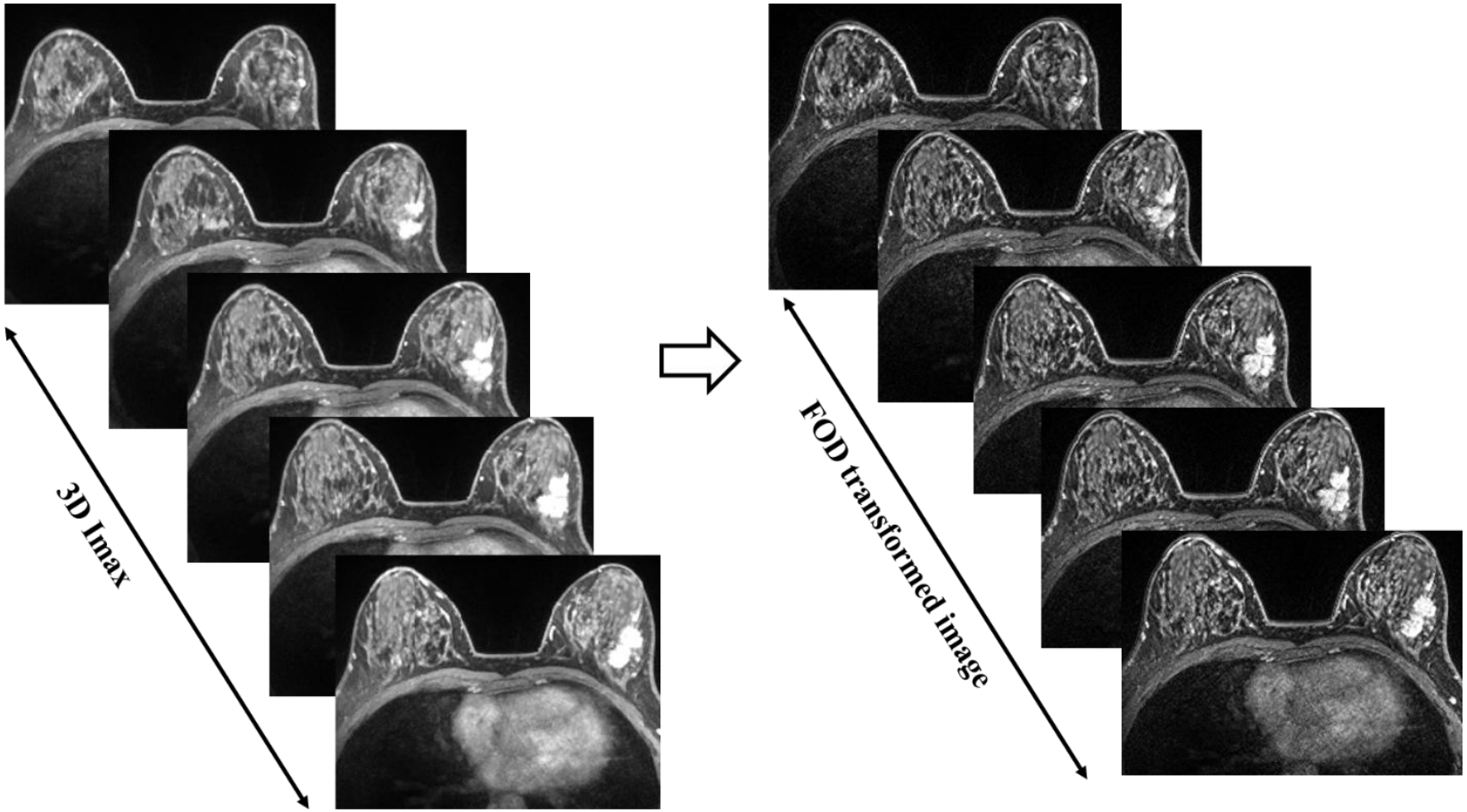

Figure 2. Visualization of 3D I_{max} and FOD-Derived Gradient Maps from DCE-MRI.

Results and Discussion

Feature Extraction Summary

Table 2. Summary of extracted radiomic features across image classes

Feature Class	Feature Split-up	Total Features
Original image class	First order: 18 Shape: 14 GLCM: 24, GLDM: 14 GLRLM: 16, GLSZM: 16 NGTDM: 5	**107**
Log filtered image (1–5 mm)	First order: 18 GLCM: 24, GLDM: 14 GLRLM: 16, GLSZM: 16 NGTDM: 5 (for each mm scale)	**93 × 5 = 465**

Results and Discussion

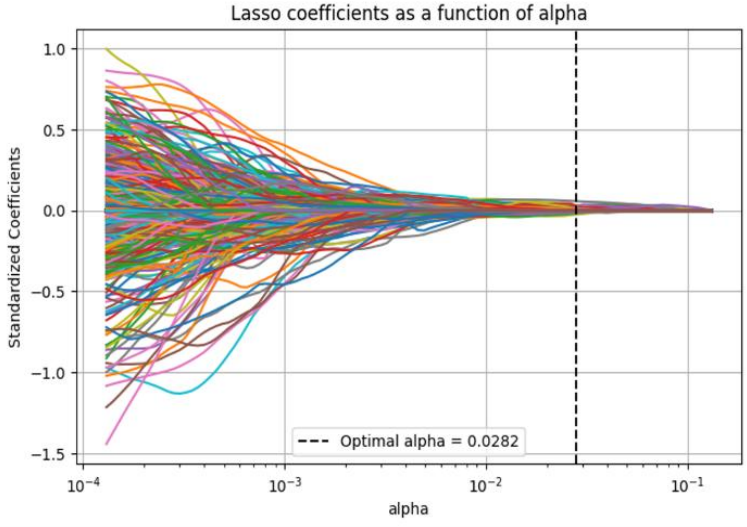

(a)

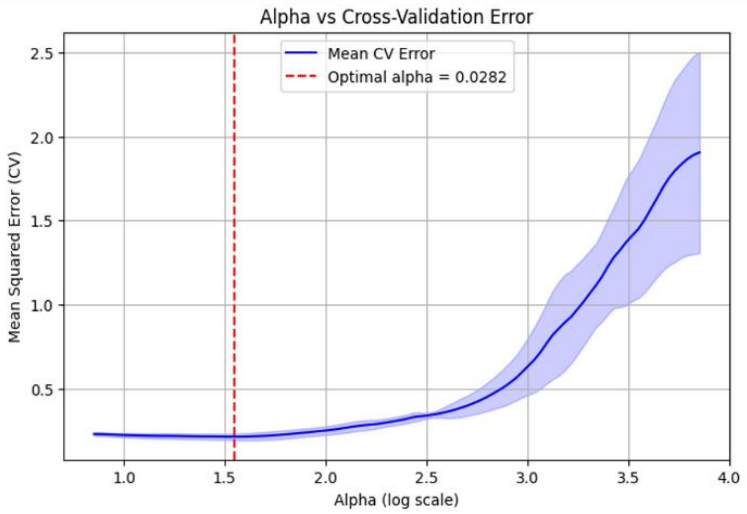

(b)

Figure 3. Visualization of LASSO regularization showing (a) Coefficient variation with α and (b) Cross-validation error for finding optimal α value.

Table 3. Feature class and category distribution of LASSO-selected features.

Feature Name	Class → Type
V1_GLNN.9	log-sigma-4-0-mm-3D → GLSZM
V1_GLV.14	log-sigma-4-0-mm-3D → GLSZM
V2_SAE.5	log-sigma-5-0-mm-3D → GLSZM
Δ_Minimum	FOD loaded image → first-order
Δ_DependenceVariance.1	log-sigma-1-0-mm-3D → GLDM
Δ_LDE.1	log-sigma-1-0-mm-3D → GLDM
Δ_RLNN.1	log-sigma-1-0-mm-3D → GLRLM
Δ_SRLGE.1	log-sigma-1-0-mm-3D → GLRLM
Δ_ZonePercentage.5	log-sigma-5-0-mm-3D → GLRLM

Results and Discussion

Table 4. Summary of tuned hyperparameters, support vectors, and model characteristics

Model	Key Hyperparameters	Support Vectors	Additional Insights
Linear SVM	C = 1.0, kernel = linear	5	Support vectors per class: [3, 2]
RBF SVM	C = 10, γ = 0.1	9	Support vectors per class: [6, 3]
Polynomial SVM	C = 1.0, degree = 3, γ = scale	6	Support vectors per class: [4, 2]
Logistic Regression	C = 1.0, penalty = L2	–	max_iter = 1000
Random Forest	n_estimators = 200, max_depth = 10	–	class_weight = balanced

Table 5. Comparative performance summary of classification models with cross-validation and statistical significance (LOOCV, n = 10)

Model	Accuracy (%)	Precision (%)	Recall (%)	F1-score (%)	p_{perm}
Linear SVM	98.4 ± 1.8 (94.1–100.0)	97.2 ± 2.6 (93.0–100.0)	96.8 ± 2.9 (91.5–100.0)	97.3 ± 2.5 (92.4–100.0)	0.048
Polynomial SVM	97.5 ± 2.4 (91.3–100.0)	96.7 ± 2.8 (91.0–100.0)	97.1 ± 2.5 (92.0–100.0)	96.9 ± 2.7 (91.2–100.0)	0.013
RBF SVM	99.2 ± 1.1 (97.2–100.0)	98.5 ± 1.6 (95.1–100.0)	99.1 ± 0.9 (97.5–100.0)	98.6 ± 1.4 (95.3–100.0)	0.020
Logistic Regression	99.3 ± 1.0 (97.0–100.0)	99.0 ± 1.2 (96.5–100.0)	99.1 ± 0.8 (97.3–100.0)	98.8 ± 1.5 (95.4–100.0)	0.029
Random Forest	99.4 ± 0.9 (97.4–100.0)	99.2 ± 1.0 (97.0–100.0)	99.3 ± 1.1 (97.2–100.0)	99.1 ± 1.0 (97.0–100.0)	0.011

Results and Discussion

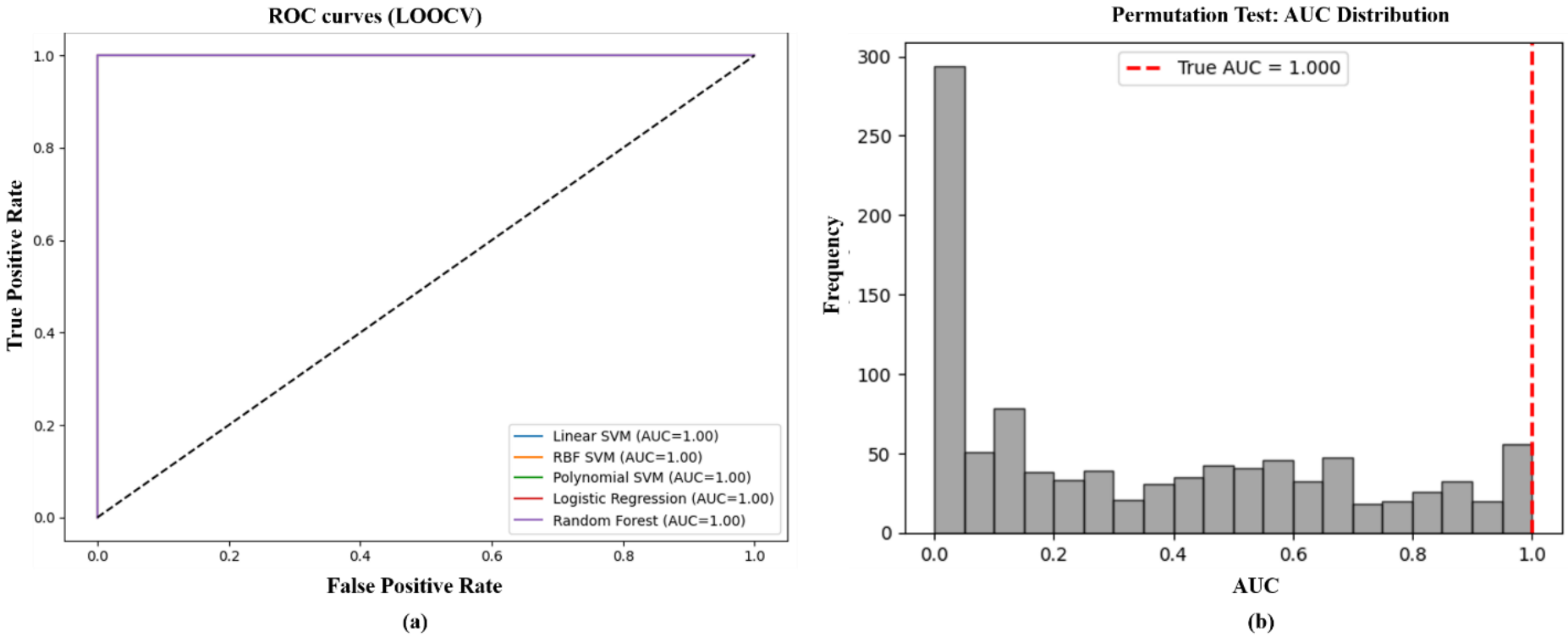

Figure 4. (a) Comparison of ROC curves for multiple classifiers. (b) Model robustness check using a permutation test.

Results and Discussion

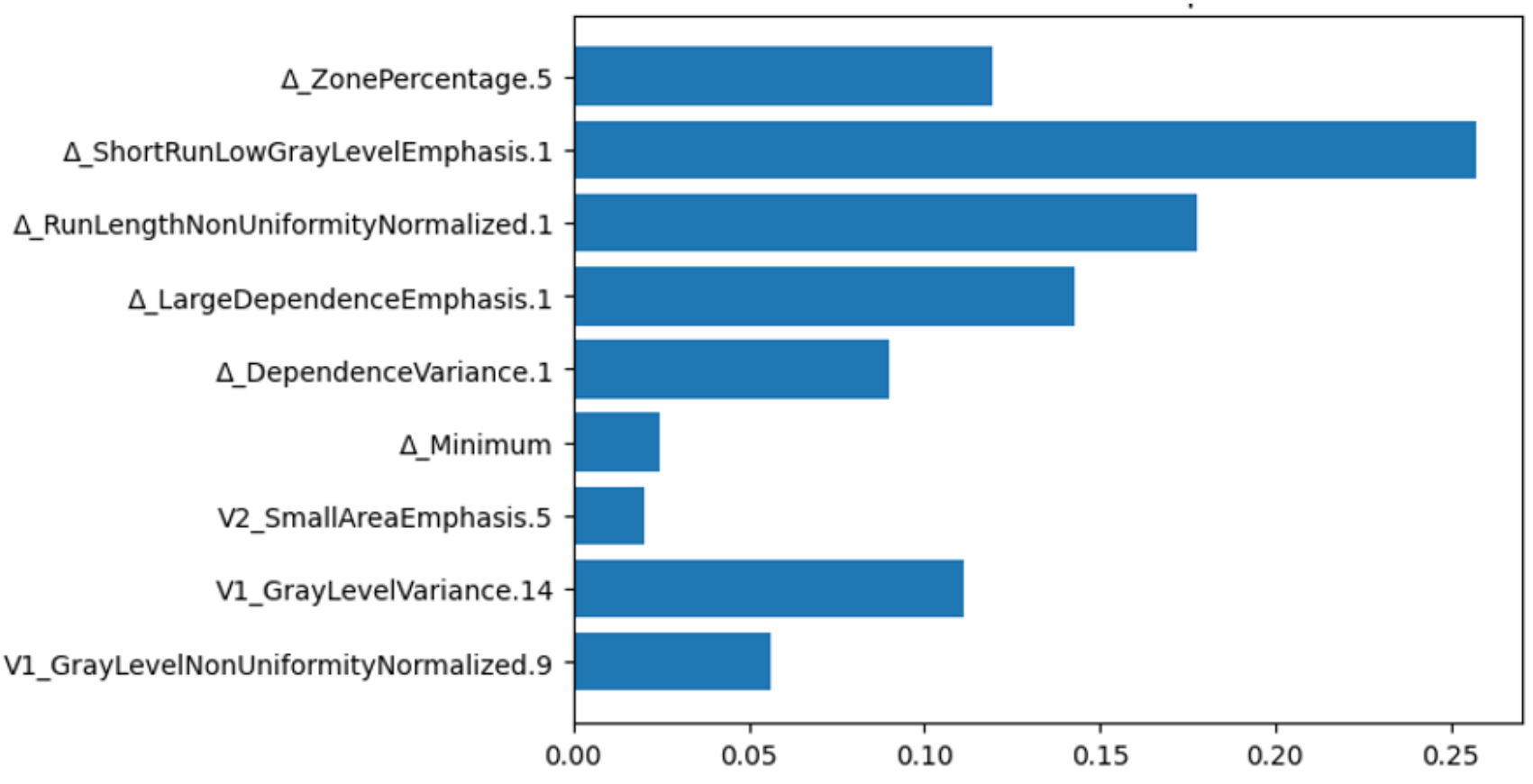

Figure 5. Feature importance of LASSO-selected features.

Limitations & Future Work

Limitations

- Small dataset (n=10), potential overfitting.
- No external validation or clinicopathological covariates.

Future Work

- Validate on larger multi-institutional cohorts.
- Integrate multi-parametric imaging and clinical data for robust prediction.

Summary

- This study presents an effective framework for classifying pCR and non-pCR patients using temporal Imax maps derived from 4D DCE-MRI.
- Fractional-order derivative (FOD) representations enhance subtle microstructural and perfusion-related tumor patterns.
- Radiomics extracted from FOD-enhanced images provide highly discriminative features for treatment response prediction.
- The combined FOD-radiomics and machine-learning approach shows strong potential for improving personalized therapy in breast cancer.

References

- R. L. Siegel, A. N. Giaquinto, and A. Jemal, “Cancer statistics, 2024.” CA: *a cancer journal for clinicians*, vol. 74, no. 1, 2024.
- M. Caballo, W. B. Sanderink, L. Han, Y. Gao, A. Athanasiou, and R. M. Mann, “Four-dimensional machine learning radiomics for the pre-treatment assessment of breast cancer pathologic complete response to neoadjuvant chemotherapy in dynamic contrast-enhanced MRI,” *Journal of Magnetic Resonance Imaging*, vol. 57, no. 1, pp. 97–110, 2023.
- J. O’connor, C. Rose, A. Jackson, Y. Watson, S. Cheung, F. Maders, B. Whitcher, C. Roberts, G. Buonaccorsi, G. Thompson et al., “DCE-MRI biomarkers of tumor heterogeneity predict CRC liver metastasis shrinkage following bevacizumab and folfox-6,” *British Journal of Cancer*, vol. 105, no. 1, pp. 139–145, 2011.
- P. Babu, M. Asaithambi, and S. M. Suriya Kumar, “Automated 3d tumor segmentation from breast DCE-MRI using energy-tuned minimax optimization,” *IEEE Access*, vol. 12, pp. 87 532–87 544, 2024.
- P. Babu, M. Asaithambi, and S. M. Suriya Kumar, “Contextual regularization-based energy optimization for segmenting breast tumor in DCE-MRI,” *IEEE Access*, 2025.

References

- J. J. Van Griethuysen, A. Fedorov, C. Parmar, A. Hosny, N. Aucoin, V. Narayan, R. G. Beets-Tan, J.-C. Fillion-Robin, S. Pieper, and H. J.Aerts, "Computational radiomics system to decode the radiographic phenotype," *Cancer research*, vol. 77, no. 21, pp. e104-e107, 2017.
- B. Priyadharshini, A. Mythili, and K. Anandh, "Performance analysis of low and high-grade breast tumors using DCE MR images and lasso feature selection," in 2023 *IEEE Signal Processing in Medicine and Biology Symposium (SPMB). IEEE*, 2023, pp. 1–6.
- E. Krasniqi, L. Filomeno, T. Arcuri, G. Ferretti, S. Gasparro, A. Fulvi, A. Roselli, L. D'Onofrio, L. Pizzuti, M. Barba et al., "Multimodal deep learning for predicting neoadjuvant treatment outcomes in breast cancer: a systematic review," *Biology Direct*, vol. 20, no. 1, p. 72, 2025.
- [14] M. Lv, B. Zhao, Y. Mao, Y. Wang, X. Su, Z. Zhang, J. Wu, X. Gao, and Q. Wang, "Deep learning model for the early prediction of pathologic response following neoadjuvant chemotherapy in breast cancer patients using dynamic contrast-enhanced MRI," *Frontiers in Oncology*, vol. 15, p. 1491843, 2025

Thank you